

Supplementary information

Alterations of the chemical profile of cholesterol in cancer tissue as traced with ToF-SIMS

Auraya Manaprasertsak^a, Julhash U. Kazi^b, Catharina Hagerling^a, Kenneth J. Pienta^c, Per Malmberg^d, and Emma U. Hammarlund^a

^aTissue Development and Evolution (TiDE), Department of Experimental Medical Sciences, Lund University, Lund, Sweden

^bDivision of Translational Cancer Research, Department of Laboratory Medicine, Lund University, Lund, Sweden

^cThe Cancer Ecology Center, Brady Urological Institute, Johns Hopkins School of Medicine, Baltimore, MD, USA.

^dDepartment of Chemistry and Chemical Engineering, Chalmers University of Technology, 412 96 Gothenburg, Sweden.

Contents:

Figure S1. The percentage ratios of various cholesterol peaks of mammary glands in whole tissue (green; n=3) and selected areas 500×500 μm² (purple; n=10). The majority of variations in isotopic patterns showed no significant distinctions between the whole tissue and the selected regions.

Figure S2. The normalized ratio of fragmented cholesterol (C₂₇H₄₅⁺: *m/z* 369) over intact cholesterol (C₂₇H₄₅O⁺: *m/z* 385) from mammary glands in WT mice (blue; n=19) and MMTV-PyMT mice (orange; n=19). Asterisks indicate a statistically significant difference with *p* < 0.0001 (****).

26 **Figure S3.** The fractional abundance from DESI-MS of **A)** fragmented cholesterol ($C_{27}H_{45}^+$: m/z
27 369) and **B)** intact cholesterol ($C_{27}H_{45}O^+$: m/z 385) from mammary glands in WT mice (blue)
28 and MMTV-PyMT mice (orange). Asterisks indicate a statistically significant difference with p
29 < 0.05 (*) and $p < 0.001$ (***)).

30 **Figure S4.** The percentage ratio of fragmented cholesterol ($C_{27}H_{45}^+$: m/z 369) over intact
31 cholesterol ($C_{27}H_{45}O^+$: m/z 385) from pure cholesterol (pink; $n=5$), mammary glands in WT
32 mice (blue; $n=19$) and MMTV-PyMT mice (orange; $n=19$). Asterisks indicate a statistically
33 significant difference with $p < 0.0001$ (****).

34 **Figure S5.** The distribution of salts (Na^+ : m/z 23 and K^+ : m/z 39) and phosphatidylcholine
35 head group ($C_5H_{12}N^+$: m/z 86 and $C_5H_{15}PNO_4^+$: m/z 184) from mammary glands from **A)** WT
36 mice and **B)** MMTV-PyMT mice.

37 **Figure S6.** The peak areas of salts (Na^+ : m/z 23 and K^+ : m/z 39) and phosphatidylcholine head
38 group ($C_5H_{12}N^+$: m/z 86 and $C_5H_{15}PNO_4^+$: m/z 184) from mammary glands from WT mice and
39 MMTV-PyMT mice.

40 **Figure S7.** The percentage ratios of various cholesterol peaks of 3 cholesterol standards. The
41 percentage ratios of each peak were labelled with the Roman numerals in **Fig. 5**.

42 **Fig. S8.** The overlay spectra in the range of m/z 366 to 370 to show the oxidation effects of **A)**
43 non-enriched cholesterol standard ($C_{27}H_{46}O$), **B)** enriched ^{13}C cholesterol standard
44 ($^{13}CC_{26}H_{46}O$) and **C)** enriched $^{13}C_2$ cholesterol standard ($^{13}C_2C_{25}H_{46}O$).

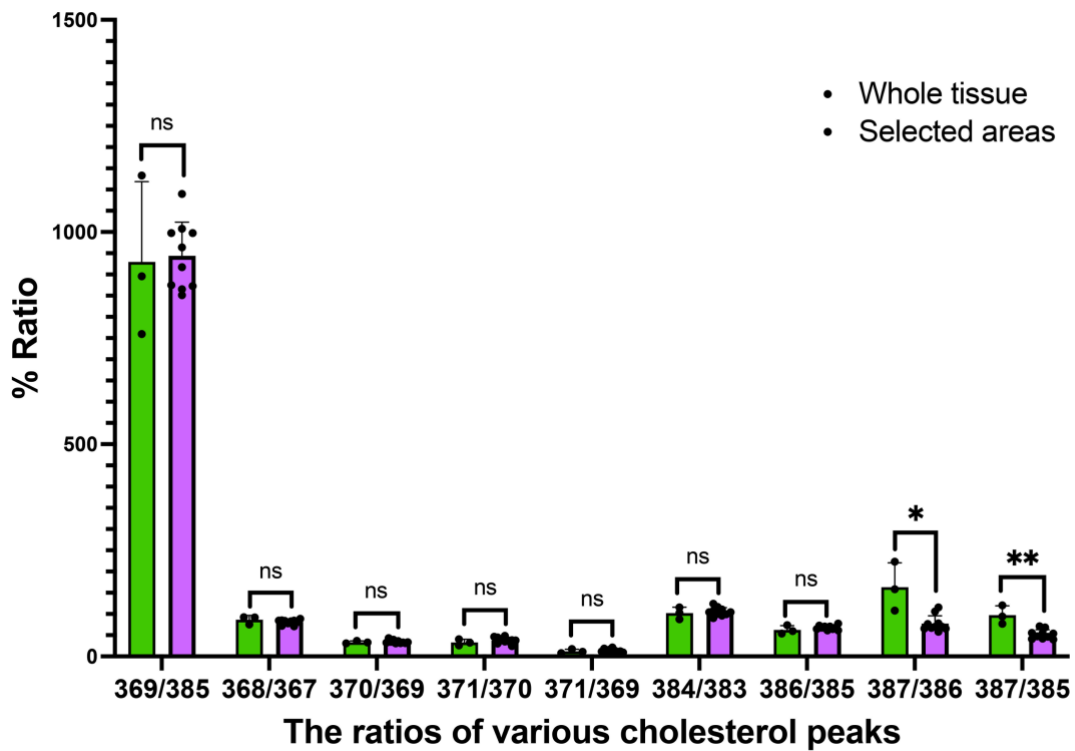
45 **Figure S9.** The normalized ratio of isotopic patterns for $^{13}CC_{26}H_{43}^+/C_{27}H_{43}^+$ (368/367),
46 $^{13}CC_{26}H_{45}^+/C_{27}H_{45}^+$ (370/369), $^{13}C_2C_{25}H_{45}^+/^{13}CC_{26}H_{45}^+$ (371/370), $^{13}C_2C_{25}H_{45}^+/C_{27}H_{45}^+$ (371/369),
47 $^{13}CC_{26}H_{43}O^+/C_{27}H_{43}O^+$ (384/383), $^{13}CC_{26}H_{45}O^+/C_{27}H_{45}O^+$ (386/385), $^{13}C_2C_{25}H_{45}O^+/^{13}CC_{26}H_{45}O^+$
48 (387/386), and $^{13}C_2C_{25}H_{45}O^+/C_{27}H_{45}O^+$ (387/385) from mammary glands in WT mice (blue;

49 n=19) and MMTV-PyMT mice (orange; n=19). Asterisks indicate a statistically significant
50 difference with $p < 0.01$ (**), $p < 0.001$ (***) and $p < 0.0001$ (****).

51 **Figure S10.** The zoom-in overlay spectra of mammary glands from **A)** and **C)** WT mouse (FVB)
52 **B)** and **D)** tumour-bearing mouse (MMTV-PyMT).

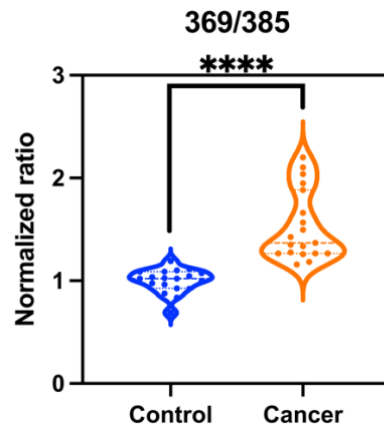
53

54 **Figure S1.** The percentage ratios of various cholesterol peaks of mammary glands in whole
55 tissue (green; n=3) and selected areas 500×500 μm² (purple; n=10). The majority of variations
56 in isotopic patterns showed no significant distinctions between the whole tissue and the
57 selected regions.
58



59
60

61 **Figure S2.** The normalized ratio of fragmented cholesterol ($C_{27}H_{45}^+$: m/z 369) over intact
62 cholesterol ($C_{27}H_{45}O^+$: m/z 385) from mammary glands in WT mice (blue; $n=19$) and MMTV-
63 PyMT mice (orange; $n=19$). Asterisks indicate a statistically significant difference with $p <$
64 0.0001 (****).

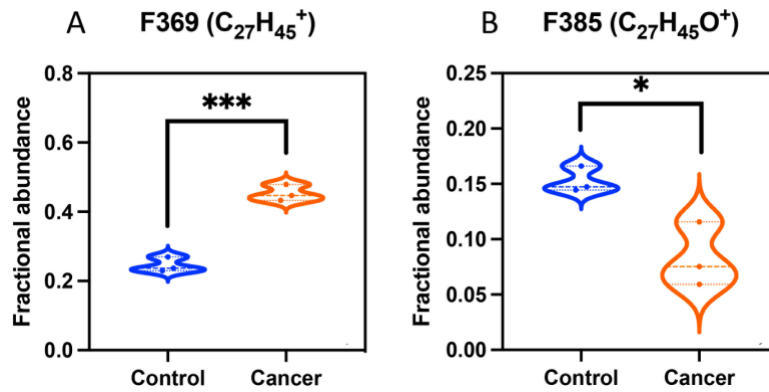


65

66

67 **Figure S3.** The fractional abundance from DESI-MS of **A**) fragmented cholesterol ($C_{27}H_{45}^+$: m/z
68 369) and **B**) intact cholesterol ($C_{27}H_{45}O^+$: m/z 385) from mammary glands in WT mice (blue)
69 and MMTV-PyMT mice (orange). Asterisks indicate a statistically significant difference with p
70 < 0.05 (*) and $p < 0.001$ (***).

71

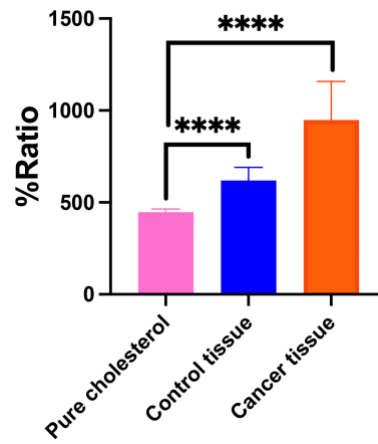


72

73

74 **Figure S4.** The percentage ratio of fragmented cholesterol ($C_{27}H_{45}^+$: m/z 369) over intact
75 cholesterol ($C_{27}H_{45}O^+$: m/z 385) from pure cholesterol (pink; $n=5$), mammary glands in WT
76 mice (blue; $n=19$) and MMTV-PyMT mice (orange; $n=19$). Asterisks indicate a statistically
77 significant difference with $p < 0.0001$ (****).

78

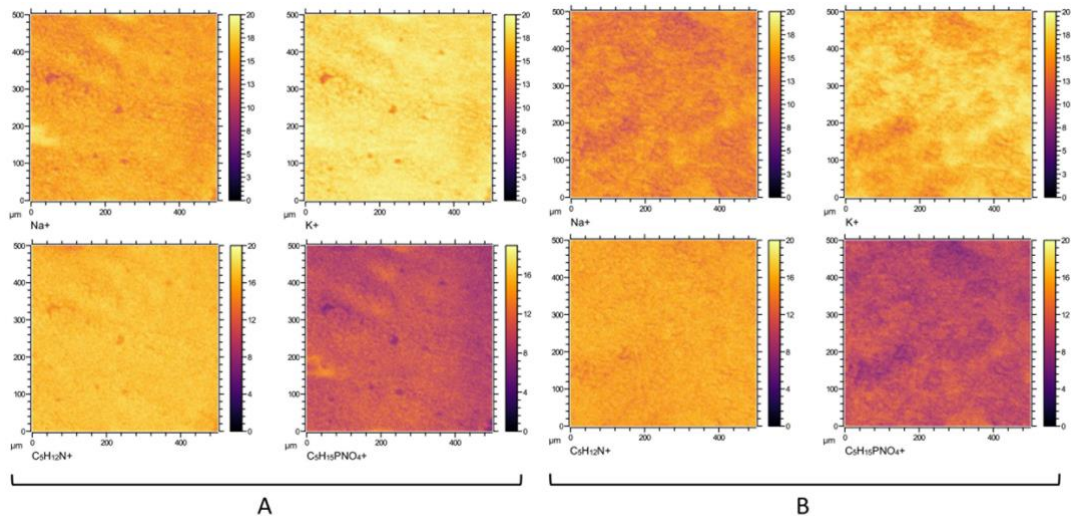


79

80

81 **Figure S5.** The distribution of salts (Na^+ : m/z 23 and K^+ : m/z 39) and phosphatidylcholine
82 head group ($\text{C}_5\text{H}_{12}\text{N}^+$: m/z 86 and $\text{C}_5\text{H}_{15}\text{PNO}_4^+$: m/z 184) from mammary glands from **A)** WT
83 mice and **B)** MMTV-PyMT mice.

84

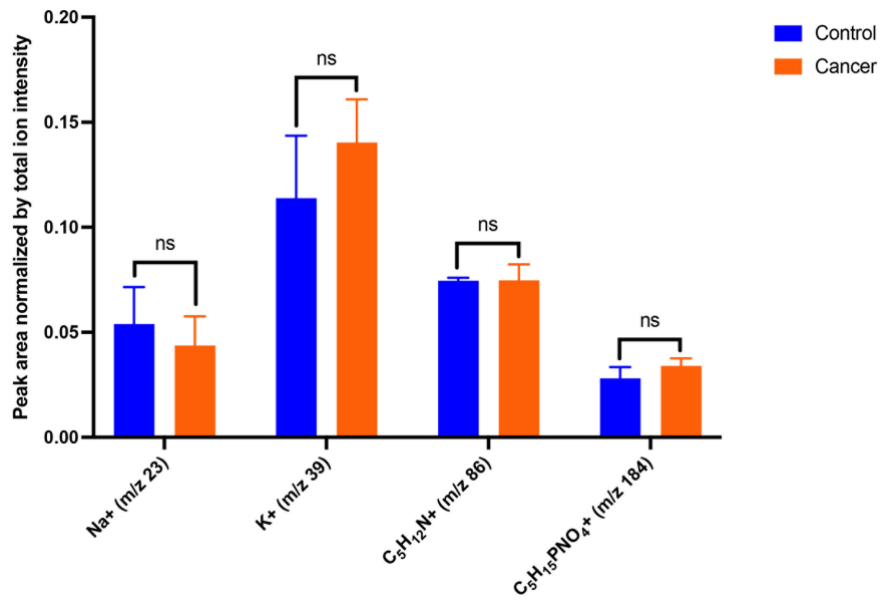


85

86

87 **Figure S6.** The peak areas of salts (Na^+ : m/z 23 and K^+ : m/z 39) and phosphatidylcholine head
88 group ($\text{C}_5\text{H}_{12}\text{N}^+$: m/z 86 and $\text{C}_5\text{H}_{15}\text{PNO}_4^+$: m/z 184) from mammary glands from WT mice and
89 MMTV-PyMT mice.

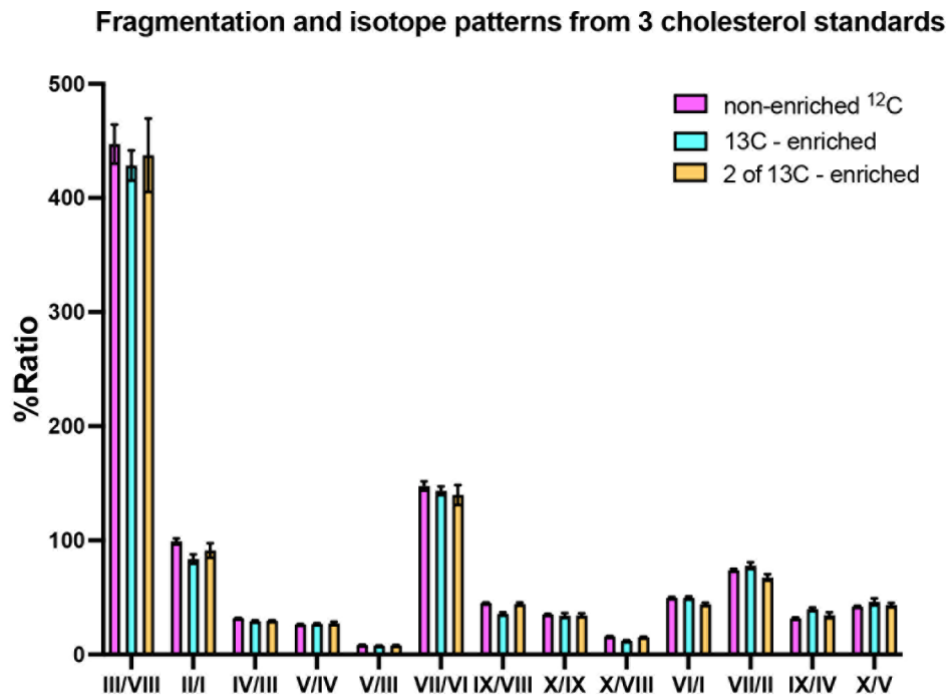
90



91

92

93 **Figure S7.** The percentage ratios of various cholesterol peaks of 3 cholesterol standards. The
94 percentage ratios of each peak were labelled with the Roman numerals in **Fig. 5**.
95

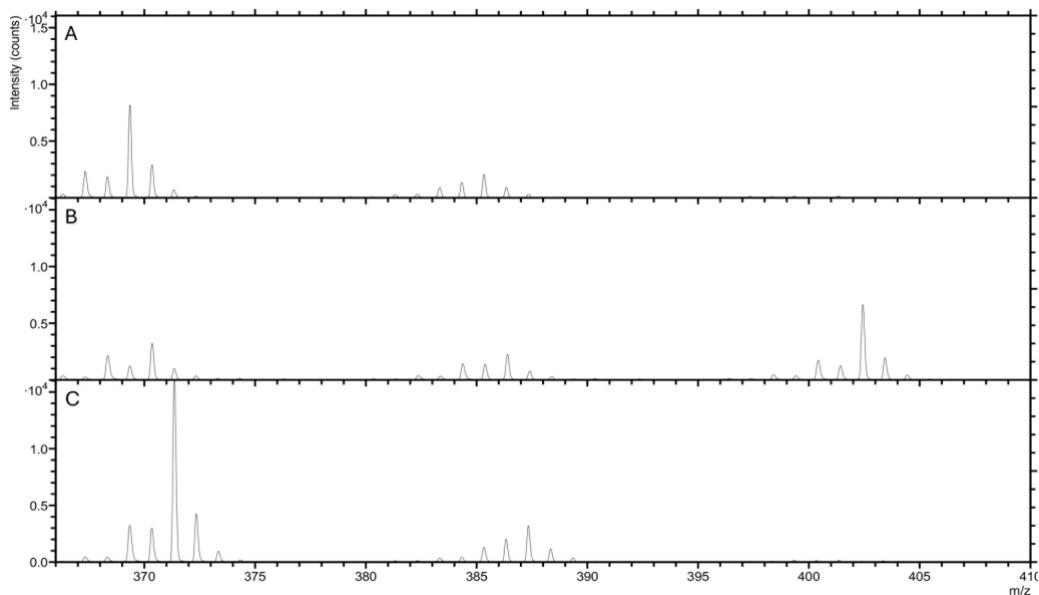


96

97

98 **Fig. S8.** The overlay spectra in the range of m/z 366 to 370 to show the oxidation effects of **A)**
99 non-enriched cholesterol standard ($C_{27}H_{46}O$), **B)** enriched ^{13}C cholesterol standard
100 ($^{13}CC_{26}H_{46}O$) and **C)** enriched $^{13}C_2$ cholesterol standard ($^{13}C_2C_{25}H_{46}O$).

101

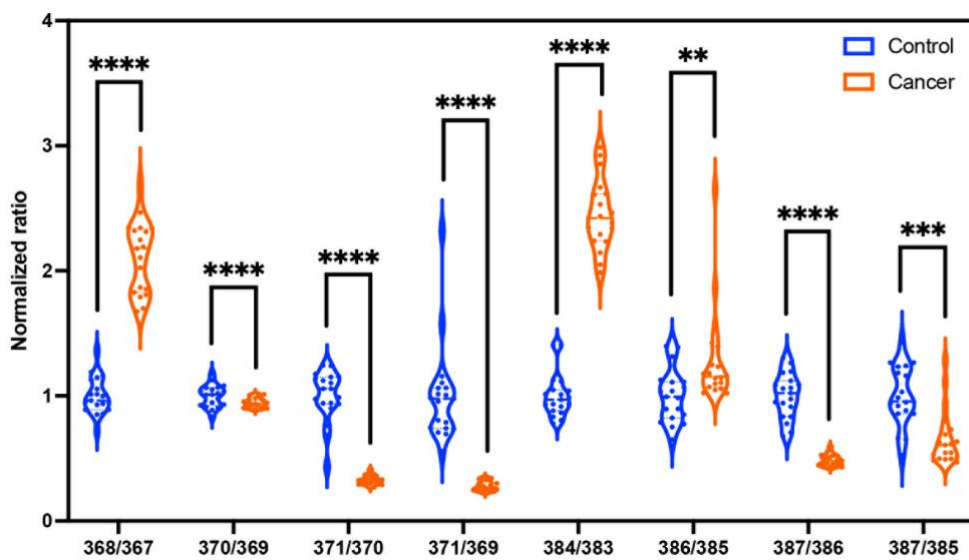


102

103

104 **Figure S9.** The normalized ratio of isotopic patterns for $^{13}\text{C}_2\text{C}_{26}\text{H}_{43}^+/\text{C}_{27}\text{H}_{43}^+$ (368/367),
 105 $^{13}\text{C}_2\text{C}_{26}\text{H}_{45}^+/\text{C}_{27}\text{H}_{45}^+$ (370/369), $^{13}\text{C}_2\text{C}_{25}\text{H}_{45}^+/\text{C}_{26}\text{H}_{45}^+$ (371/370), $^{13}\text{C}_2\text{C}_{25}\text{H}_{45}^+/\text{C}_{27}\text{H}_{45}^+$ (371/369),
 106 $^{13}\text{C}_2\text{C}_{26}\text{H}_{43}\text{O}^+/\text{C}_{27}\text{H}_{43}\text{O}^+$ (384/383), $^{13}\text{C}_2\text{C}_{26}\text{H}_{45}\text{O}^+/\text{C}_{27}\text{H}_{45}\text{O}^+$ (386/385), $^{13}\text{C}_2\text{C}_{25}\text{H}_{45}\text{O}^+/\text{C}_{26}\text{H}_{45}\text{O}^+$
 107 (387/386), and $^{13}\text{C}_2\text{C}_{25}\text{H}_{45}\text{O}^+/\text{C}_{27}\text{H}_{45}\text{O}^+$ (387/385) from mammary glands in WT mice (blue;
 108 n=19) and MMTV-PyMT mice (orange; n=19). Asterisks indicate a statistically significant
 109 difference with $p < 0.01$ (**), $p < 0.001$ (***) and $p < 0.0001$ (****).

110

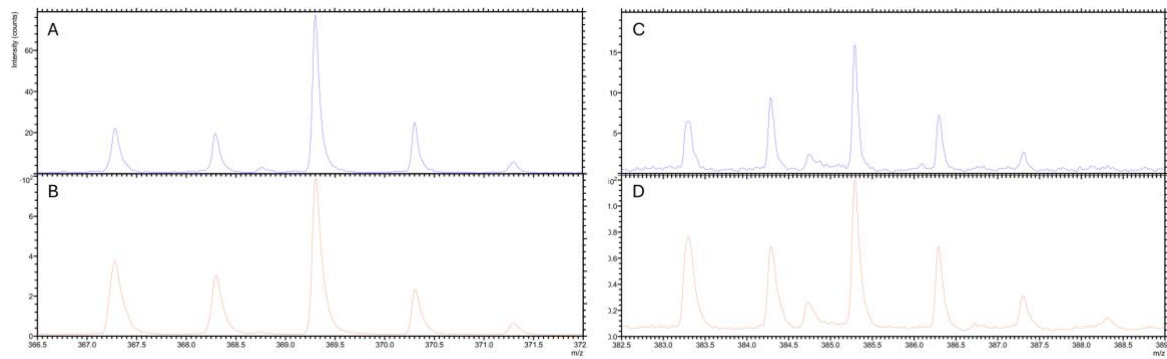


111

112

113 **Figure S10.** The zoom-in overlay spectra of mammary glands from **A)** and **C)** WT mouse (FVB)
114 **B)** and **D)** tumour-bearing mouse (MMTV-PyMT).

115



116